Received: 28 May 2020 | Revised: 10 July 2020 | Accepted: 21 July 2020

DOI: 10.1111/jace.17393



Journal of the American Ceramic Society

ORIGINAL ARTICLE

# Inversion of quartz solid solutions at cryogenic temperatures

**Alessio Zandona** | **Gundula Helsch** | **Joachim Deubener**

Institute of Non-Metallic Materials, Clausthal University of Technology, Clausthal-Zellerfeld, Germany

**Correspondence**
Alessio Zandona, Institute of Non-Metallic Materials, Clausthal University of Technology, Clausthal-Zellerfeld, Germany.
Email: alessio.zandona@tu-clausthal.de

**Abstract**

Quartz solid solution crystals of six different compositions were obtained from crystallization of glass powders belonging to the $Li_2O$–$Al_2O_3$-$SiO_2$ (LAS) system. They were analyzed in situ by laboratory-based X-ray diffraction down to cryogenic temperatures (−190°C). Temperature-resolved analysis of their lattice parameters allowed determination of the critical inversion temperature $T_c$ in these materials, marking the displacive phase transition from a high-quartz- to a low-quartz-like lattice. Integrating available data from other literature sources, an updated phase diagram for the occurrence of high and low quartz solid solution phases is provided for the LAS system; these data are expected to support future development of functional materials relying on these crystalline phases.

**KEYWORDS**

cryogenics, LAS glass-ceramics, quartz inversion, quartz solid solution, X-ray diffraction

## 1 | INTRODUCTION

The occurrence of stuffed derivatives[1] of the low ($P3_121$ or $P3_221$) and high ($P6_422$ or $P6_222$) quartz (or α- and β-quartz) structures[2] has been known in the $Li_2O$–$Al_2O_3$-$SiO_2$ (LAS) compositional system since the early crystallographic investigation of synthetic high- or β-eucryptite[3] ($LiAlSiO_4$) prepared from crystallized glasses. Shortly after, dilatometric investigations revealed that these materials can exhibit low or even negative thermal expansion over a wide temperature range.[4] This discovery awakened a long-lasting scientific and technological interest that particularly boomed after the development of glass-ceramics.[5] Opaque and transparent zero-thermal-expansion glass-ceramics are indeed still produced today based on LAS compositions.[6,7]

Although only compositions close to the $LiAlSiO_4$ end-member display thermodynamic stability at room temperature and pressure,[8] these stuffed derivatives can be synthesized metastably down to the pure $SiO_2$ end-member[9-11]; their natural occurrence is conversely rather rare.[12] Denominations such as β-eucryptite solid solution and quartz solid solution (Qss) are widespread in the literature and the latter one will be preferred in the following, since it allows a further structural distinction between low-quartz- or high-quartz-like lattice (hereafter LQss and HQss, respectively). Indeed, the Li ions occupy tetrahedral sites in the otherwise hollow channels running parallel to the c-direction in the quartz structure, whereas Al partially substitutes Si in the tetrahedral silicate framework, composed by six- and eight-membered rings.[3,13] At a critical composition, previously located at a $SiO_2$ crystal content of ~83 mol%,[14] the structural stuffing is able to stabilize the less dense hexagonal structure of high quartz[15] down to room temperature. Recent investigations of the α-β inversion temperature $T_c$, conventionally fixed at 573°C in pure quartz,[16] have indicated its overall linear decrease down to cryogenic temperatures as a function of increasing Al- and Li-incorporation in the crystals.[17,18] This observation, though in accordance with previous theoretical predictions,[19] was based on a single $T_c$ data point for temperatures below ambient,[17] due to the special instrumentation

**TABLE 1** Nominal molar composition of the employed glass samples and of the resulting Qss crystals

| Sample | Glass | | | Qss stoichiometry | Crystallization temperature (°C) |
|---|---|---|---|---|---|
| | $Li_2O$ (mol%) | $Al_2O_3$ (mol%) | $SiO_2$ (mol%) | | |
| LA222 | 12.21 | 10.96 | 76.83 | 1 $Li_2O$ · 1 $Al_2O_3$ · 7.00 $SiO_2$ | 760 |
| LA213 | 11.72 | 10.52 | 77.76 | 1 $Li_2O$ · 1 $Al_2O_3$ · 7.39 $SiO_2$ | 780 |
| LA204 | 11.22 | 10.08 | 78.70 | 1 $Li_2O$ · 1 $Al_2O_3$ · 7.80 $SiO_2$ | 800 |
| LA195 | 10.73 | 9.64 | 79.63 | 1 $Li_2O$ · 1 $Al_2O_3$ · 8.25 $SiO_2$ | 800 |
| LA186 | 10.23 | 9.20 | 80.57 | 1 $Li_2O$ · 1 $Al_2O_3$ · 8.75 $SiO_2$ | 820 |
| LA177 | 9.73 | 8.76 | 81.50 | 1 $Li_2O$ · 1 $Al_2O_3$ · 9.30 $SiO_2$ | 820 |

required at these challenging conditions. Note that Qss phases can be also obtained if Mg and Zn are employed as stuffing cations instead of Li.[10,11,20-23] Particularly in the case of Mg doping, however, the univocal assignment of their structure to a high or low quartz symmetry is still debated.[24-26]

This study was designed as a targeted investigation of the α-β inversion temperature $T_c$ at stoichiometries marking the structural transition between room-temperature-stabilized HQss and LQss in the LAS compositional system. In situ measurements at cryogenic temperatures (down to −190°C) were performed on a laboratory-based equipment and were used to integrate the available data from other literature sources. All in all, the results of this work definitively pinpoint the domains of LQss and HQss occurrence in the LAS system as a function of temperature and chemical composition.

## 2 | EXPERIMENTAL PROCEDURE

### 2.1 | Sample preparation

The compositions of the six glass samples used for this study are shown in Table 1. They were selected based on the results of previous investigations of Li-bearing Qss phases,[17,18] in order to obtain crystalline products with α-β inversion temperatures located below ambient. An excess of 10% $Li_2O$ was added to compensate for potential losses during melting and ensure that the molar ratio Al/Li ≤ 1, so that the Qss crystals could then form according to the targeted Al/Si ratios. Furthermore, the $Li_2O$ addition reduced the viscosity and facilitated pouring of the glass melts. These were produced from a mixture of $Al(OH)_3$, $Li_2CO_3$, and $SiO_2$ raw materials, melted at 1600°C in fused silica crucibles and then quenched on a cold steel plate, respectively, obtaining ~50 g of transparent glass.

The glasses were ground into powder and devitrified in a diffractometer (Empyrean, Malvern Panalytical), equipped with a high-temperature chamber (HTK 1200 N, Anton Paar). This allowed to monitor the crystallization process in situ: the samples were heated up until satisfactory amounts of Qss crystals had formed (crystallization temperatures are reported in Table 1) and then rapidly cooled, to avoid complete transformation into keatite solid solution (Kss), the thermodynamically stable phase at these compositions.[8] In fact, the formation of Kss started inevitably and promptly after the first appearance of Qss, far before full crystallization of the

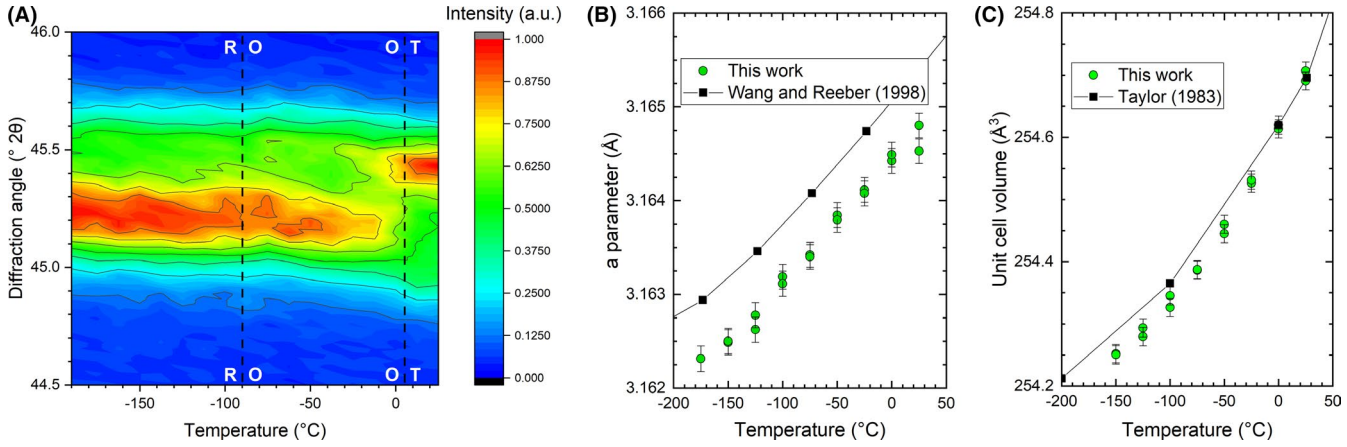


**FIGURE 1** Results of preliminary tests of the XRD cooling chamber: (A) intensity variation in the diffraction pattern of $BaTiO_3$ in the range 44.5-46 °2θ due to structural phase transitions at approximately 5°C and −90°C[27] (T for tetragonal, O for orthorhombic and R for rhombohedral structure); (B) *a* lattice parameter of metallic tungsten W and (C) unit cell volume of $Al_2O_3$ (SRM676) at temperatures between 25°C and −175°C, in comparison to respective references.[28,29] [Color figure can be viewed at wileyonlinelibrary.com]

glasses: several attempts were therefore conducted to maximize the Qss content of all samples, which still eventually contained roughly 30-50 wt% Kss (neglecting minor amounts of uncrystallised glass).

## 2.2 | X-ray diffraction (XRD) at room temperature

The crystallized powders were measured in Bragg-Brentano geometry in the above-mentioned diffractometer operated at 40 mA/ 40 kV and equipped with a copper X-ray tube, an adjustable x-y-z stage with a powder sample holder and a PIXcel 1D detector (255 channels, 14 mm active length). The incident beam optics included: a 0.125° divergence slit, a 4 mm mask, a BBHD mirror, 0.04 mm Soller slits and a 0.5° antiscatter slit. The diffracted beam optics included: a 7.5 mm antiscatter slit and 0.04 mm Soller slits. The measurements were performed in the 10-90 °2θ range with a step size of 0.026 °2θ, 50 seconds per step and a total duration of approximately 10 minutes. The lattice parameters of Qss were obtained from Rietveld refinements, using the software HighScore Plus (Malvern Panalytical).

## 2.3 | X-ray diffraction (XRD) at cryogenic temperatures

Nonambient XRD measurements at cryogenic temperatures were performed on the above-mentioned diffractometer, equipped with a TTK 600 chamber (Anton Paar) operated with liquid $N_2$ cooling under vacuum ($10^{-2}$ mbar). The reliability of its operation was tested through the measurement of some standard materials ($BaTiO_3$ powder, Alfa Aesar; metallic W powder, Alfa Aesar; $Al_2O_3$ powder, NIST SRM676). The values obtained for the phase transformation temperatures in $BaTiO_3$ (Figure 1A) and for the thermal expansion of W and $Al_2O_3$ (Figure 1B,C) adequately matched those expected from literature sources.[27-29] However, the determined lattice constants occasionally deviated from the ideal values. This effect was ascribed inter alia to imperfect sample alignment (see below for details on sample preparation) and corrected by introducing a weighed-in silicon powder standard in the analyzed samples.

To ensure the best possible heat transfer between sample holder and powder, approximately 100 mg of crystallized LAS powder and 5-10 mg of Si standard were mixed with some Apiezon N cryogenic vacuum grease (Demaco) until obtaining a dense homogeneous paste. A thin layer of this paste was then applied to a flat temperature-controlled metallic sample holder and measured during cooling between 25°C and −190°C in 12.5°C temperature intervals. For comparative purposes, some measurements were performed also during the subsequent heating ramp in 50 K intervals. The diffractometer optics corresponded to the ones used at room temperature, whereas the measurements were performed in the range 15-90 °2θ with a step size of 0.026 °2θ, 20 seconds per step and total duration of approximately 5 minutes. The lattice parameters of Qss were again obtained using the software HighScore Plus (Malvern Panalytical).

# 3 | RESULTS

All analyzed glass powders could be crystallized into Qss, although they also inevitably developed non-negligible amounts of Kss (Figure 2A). The early occurrence of this

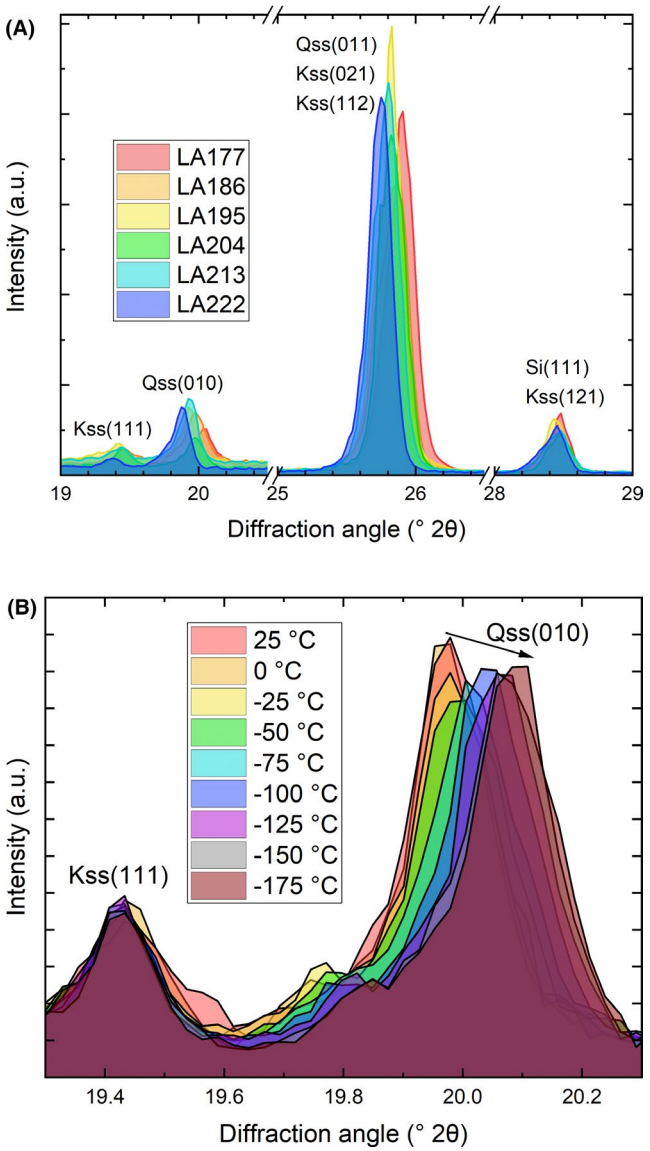


**FIGURE 2** Selected (hkl)-reflections of the diffraction measurements performed in the XRD cooling chamber: (A) all analyzed LAS powders at room temperature and (B) sample LA186 between 25°C and −175°C (Qss for quartz solid solution, Kss for keatite solid solution, Si for the weighed-in silicon standard) [Color figure can be viewed at wileyonlinelibrary.com]

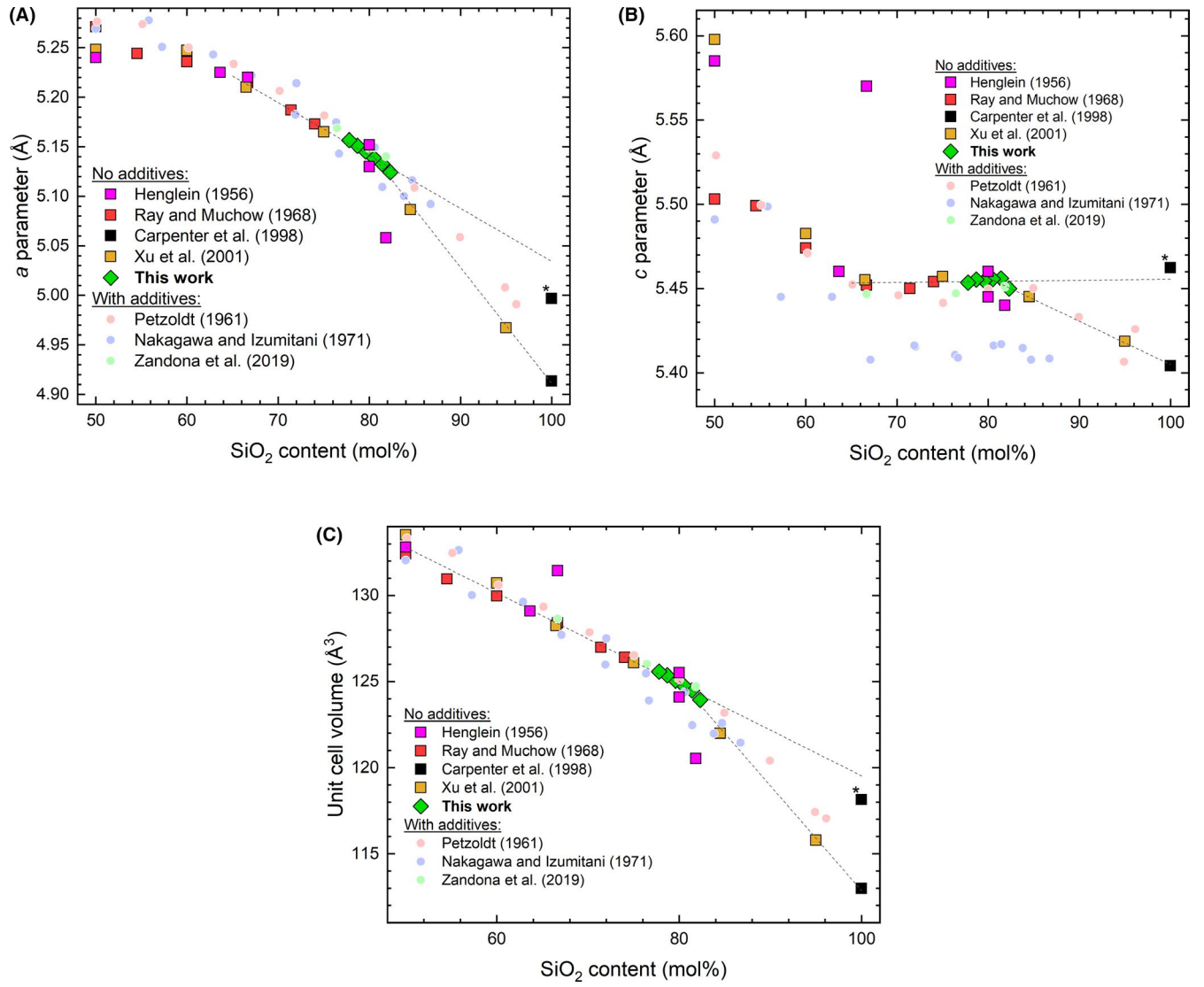


**FIGURE 3** A, *a* lattice constant, (B) *c* lattice constant, and (C) unit cell volume of Qss as obtained at room temperature for all analyzed LAS crystals, plotted against their nominal $SiO_2$ content and in comparison with various literature sources[9-11,14,22,30,32] (* labels the lattice parameters of pure high quartz extrapolated to room temperature). The data from Ray and Muchow (1968), Carpenter et al (1998), Xu et al (2001) and this work were used for linear interpolation. If not indicated, error bars are smaller than the depicted symbols [Color figure can be viewed at wileyonlinelibrary.com]

phase was not unexpected due to its thermodynamic stability at these compositions[8] and was in accordance with previous results in $TiO_2$-nucleated glass-ceramics.[22] Moreover, the formation of Kss did not appear to induce undesired compositional shifts of the Qss phases, whose lattice parameters at room temperature matched the values expected from literature sources (Figure 3). These previous works invariably obtained Qss by devitrification with the exception of Henglein[9] and Carpenter et al,[30] who examined naturally occurring crystals, and Xu et al,[14] who also employed high-temperature sintering and high-temperature high-pressure protocols.[31] Concerning additional data points from glass-ceramics containing nucleating agents (typically $TiO_2$ and $ZrO_2$[10,22,32]), they are more scattered, but show a general agreement with the trend of stoichiometric references (square points in the figure). Notice that all points are plotted according to the nominal composition of the obtainable Qss crystals in the samples (Table 1), as most of the other authors did before us.

Both *a* and *c* lattice parameters display an overall complex behavior previously ascribed to two main structural transitions,[14] namely: 1) a continuous Al-Si order-disorder transition at $SiO_2$ = ~65 mol%, due to the gradual compositional weakening of Löwenstein's energetic requirements[33] starting from the $LiAlSiO_4$ end-member; 2) a more abrupt discontinuity at $SiO_2$ = ~83 mol%, marking the inversion from a high-quartz-like to a low-quartz-like symmetry. Only this latter phenomenon clearly affected the unit cell volume of the crystals, as manifested by the two linear interpolations for the HQss and LQss regimes in Figure 3C. The samples analyzed within

**TABLE 2** Lattice parameters *a* of Qss as obtained from XRD measurements at cryogenic temperatures in all studied powders; numbers in parentheses provide the uncertainty of the last digits

| | Samples | | | | | |
|---|---|---|---|---|---|---|
| T (°C) | LA222 | LA213 | LA204 | LA195 | LA186 | LA177 |
| 25.0 | 5.1544(4) | 5.1486(5) | 5.1455(6) | 5.1394(5) | 5.1315(6) | 5.1238(6) |
| 12.5 | 5.1544(4) | 5.1486(5) | 5.1459(6) | 5.1391(5) | 5.1315(6) | 5.1236(6) |
| 0.0 | 5.1543(4) | 5.1487(5) | 5.1459(6) | 5.1392(5) | 5.1305(7) | 5.1222(7) |
| −12.5 | 5.1542(4) | 5.1488(5) | 5.1460(6) | 5.1387(5) | 5.1309(7) | 5.1200(7) |
| −25.0 | 5.1543(4) | 5.1489(5) | 5.1462(6) | 5.1387(5) | 5.1294(7) | 5.1177(7) |
| −37.5 | 5.1540(4) | 5.1489(5) | 5.1461(6) | 5.1383(5) | 5.1280(7) | 5.1161(7) |
| −50.0 | 5.1542(4) | 5.1490(5) | 5.1461(6) | 5.1375(5) | 5.1273(8) | 5.1125(7) |
| −62.5 | 5.1540(4) | 5.1487(5) | 5.1457(6) | 5.1368(5) | 5.1252(8) | 5.1119(7) |
| −75.0 | 5.1540(4) | 5.1485(5) | 5.1455(6) | 5.1358(5) | 5.1198(8) | 5.1077(7) |
| −87.5 | 5.1539(4) | 5.1484(5) | 5.1450(6) | 5.1343(5) | 5.1167(8) | 5.1072(7) |
| −100.0 | 5.1536(4) | 5.1483(5) | 5.1443(7) | 5.1314(5) | 5.1152(8) | 5.1040(7) |
| −112.5 | 5.1537(5) | 5.1480(5) | 5.1433(7) | 5.1265(5) | 5.1135(8) | 5.1041(7) |
| −125.0 | 5.1533(5) | 5.1477(5) | 5.1420(7) | 5.1228(5) | 5.1122(8) | 5.1020(7) |
| −137.5 | 5.1532(5) | 5.1469(6) | 5.1391(7) | 5.1204(5) | 5.1104(7) | 5.1002(7) |
| −150.0 | 5.1530(5) | 5.1464(6) | 5.1389(7) | 5.1199(5) | 5.1101(8) | 5.0991(7) |
| −162.5 | 5.1527(5) | 5.1448(6) | 5.1359(7) | 5.1183(5) | 5.1088(7) | 5.0985(7) |
| −175.0 | 5.1521(5) | 5.1430(6) | 5.1344(7) | 5.1172(5) | 5.1075(7) | 5.0971(7) |
| −190.0 | 5.1512(5) | 5.1410(6) | 5.1317(7) | 5.1155(5) | 5.1064(7) | 5.0955(7) |
| −150.0 | 5.1531(5) | 5.1461(6) | 5.1389(7) | 5.1183(5) | 5.1091(8) | 5.0988(7) |
| −100.0 | 5.1538(5) | 5.1481(5) | 5.1446(6) | 5.1306(5) | 5.1128(8) | 5.1030(7) |
| −50.0 | 5.1541(4) | 5.1488(5) | 5.1462(6) | 5.1378(5) | 5.1267(8) | 5.1110(7) |
| 0.0 | 5.1542(4) | 5.1486(5) | 5.1464(6) | 5.1387(5) | 5.1302(7) | 5.1211(7) |
| 25.0 | 5.1542(4) | 5.1485(5) | 5.1461(6) | 5.1387(5) | 5.1309(6) | 5.1242(6) |

this study are located exactly in this transitional region: they all aligned with the HQss trend, apart from LA177 (nominal $SiO_2 = 82.3$ mol%), whose structural parameters started to approach the ones expected for a LQss lattice.

The lattice constants obtained during in situ measurements between 25°C and −190°C are reported in the Tables 2 and 3 and in Figure 4. In consistency with previous considerations, the single *a*-curves were sensibly staggered over the vertical axis, whereas the *c* parameter was again only limitedly influenced by compositional variations, especially in this stoichiometric range. Two thermal expansion regimes were visible in both graphs: positive thermal expansion at cryogenic temperatures, corresponding to LQss, was invariably associated with a null or slightly negative one up to 25°C, assignable to HQss. They were linked by a somehow gradual transition interval that shifted to higher temperatures with increasing $SiO_2$ content of the samples, until it resulted barely visible in the Si-richer LA177. The volumetric expansion of the crystals (Figure 5) provides similar insights and effectively integrates the data published by other authors.[17]

Critical inversion temperatures $T_c$ were extracted from these data by the double-tangent method (Table 4). The interdependence between $T_c$ and $SiO_2$ content appeared to be linear (Figure 6), as previously postulated by theoretical calculations.[19] Consequently, the essential agreement between the data determined within this work and the results of Xu et al[17] enabled the compilation of a comprehensive diagram of the LQss–HQss relations in the LAS system. The $T_c$ values reported previously for sol-gel derived thin films plotted systematically higher than the ones obtained from bulk samples: they might be affected by crystallization-induced stress fields.[18]

## 4 | DISCUSSION

The Qss structural parameters and inversion temperatures $T_c$ determined in this work display an excellent agreement with previous literature sources. This is rather surprising if one considers the time span and the range of analytical developments that have taken place since the first investigations performed by Henglein in 1956.[9] The results obtained in this work using

**TABLE 3** Lattice parameters *c* of Qss as obtained from XRD measurements at cryogenic temperatures in all studied powders; numbers in parentheses provide the uncertainty of the last digits

| | Samples | | | | | |
|---|---|---|---|---|---|---|
| *T* (°C) | LA222 | LA213 | LA204 | LA195 | LA186 | LA177 |
| 25.0 | 5.4535(6) | 5.4544(7) | 5.4568(9) | 5.4519(7) | 5.4575(8) | 5.4518(8) |
| 12.5 | 5.4538(6) | 5.4547(7) | 5.4551(8) | 5.4525(7) | 5.4575(8) | 5.4494(9) |
| 0.0 | 5.4547(6) | 5.4544(7) | 5.4553(8) | 5.4529(6) | 5.4578(8) | 5.4484(10) |
| −12.5 | 5.4550(6) | 5.4545(7) | 5.4550(8) | 5.4534(6) | 5.4574(8) | 5.4469(9) |
| −25.0 | 5.4551(6) | 5.4547(7) | 5.4550(8) | 5.4533(6) | 5.4580(9) | 5.4457(10) |
| −37.5 | 5.4557(6) | 5.4546(7) | 5.4550(8) | 5.4538(6) | 5.4581(9) | 5.4450(10) |
| −50.0 | 5.4562(6) | 5.4548(7) | 5.4551(8) | 5.4543(7) | 5.4571(9) | 5.4453(10) |
| −62.5 | 5.4564(6) | 5.4547(7) | 5.4551(8) | 5.4543(7) | 5.4571(9) | 5.4433(10) |
| −75.0 | 5.4564(6) | 5.4551(7) | 5.4548(9) | 5.4544(7) | 5.4551(9) | 5.4438(9) |
| −87.5 | 5.4567(6) | 5.4551(7) | 5.4546(9) | 5.4539(7) | 5.4542(9) | 5.4431(9) |
| −100.0 | 5.4571(6) | 5.4552(7) | 5.4545(9) | 5.4532(7) | 5.4520(10) | 5.4426(9) |
| −112.5 | 5.4571(6) | 5.4550(7) | 5.4540(10) | 5.4527(6) | 5.4516(9) | 5.4414(9) |
| −125.0 | 5.4574(6) | 5.4546(7) | 5.4518(10) | 5.4522(6) | 5.4507(9) | 5.4415(9) |
| −137.5 | 5.4578(6) | 5.4543(7) | 5.4518(10) | 5.4521(6) | 5.4503(9) | 5.4409(9) |
| −150.0 | 5.4576(6) | 5.4535(8) | 5.4499(10) | 5.4502(6) | 5.4495(9) | 5.4412(9) |
| −162.5 | 5.4577(7) | 5.4530(8) | 5.4516(10) | 5.4506(6) | 5.4490(9) | 5.4404(9) |
| −175.0 | 5.4576(7) | 5.4519(8) | 5.4515(10) | 5.4501(6) | 5.4480(9) | 5.4408(9) |
| −190.0 | 5.4577(7) | 5.4517(9) | 5.4523(9) | 5.4492(6) | 5.4478(9) | 5.4402(9) |
| −150.0 | 5.4578(6) | 5.4535(8) | 5.4500(10) | 5.4517(6) | 5.4496(9) | 5.4409(9) |
| −100.0 | 5.4576(6) | 5.4548(7) | 5.4548(9) | 5.4548(7) | 5.4533(9) | 5.4437(9) |
| −50.0 | 5.4562(6) | 5.4542(7) | 5.4547(8) | 5.4541(7) | 5.4568(9) | 5.4455(9) |
| 0.0 | 5.4547(6) | 5.4534(7) | 5.4544(8) | 5.4534(6) | 5.4567(8) | 5.4477(9) |
| 25.0 | 5.4544(6) | 5.4533(7) | 5.4542(8) | 5.4532(7) | 5.4567(7) | 5.4512(8) |

a laboratory-based cryogenic equipment substantially overlap with those produced at large-scale facilities[17] and therefore represent a promising and undemanding approach for future investigations in the field of in situ X-ray diffraction.

For the whole treatment, the Al/Si ratio of the Qss crystals was assumed equal to the initial stoichiometry of the glass (their composition was indeed recalculated neglecting the $Li_2O$ excess of the glasses, see Table 1). All literature sources summarized in Figure 3 adopted this same method with the exception of Xu et al,[17] who reported the occasional coexistence of several Qss variants after high-temperature high-pressure synthesis and tried to correct for it. In our samples, even the structural parameters of Kss (30-50 wt% of the crystalline fraction) display a clear linear dependence from the nominal composition, with a strikingly good agreement with the available literature sources, as shown in Figure 7. This observation suggests that both Qss and Kss precipitated almost simultaneously in a viscous melt that did not allow any major chemical enrichment by diffusion, as it is probably the case at the relatively low temperatures (and therefore high viscosities) selected for the heat treatments. Following these views, the Al/Si ratio of the initial glass appears to be the crucial factor determining the stoichiometry of the resulting Qss and Kss crystals, being also necessarily maintained in the remaining amorphous phase throughout the crystallization.

Concerning the data points pertaining to glass-ceramics containing crystallization additives (Figure 3), a higher scattering of the values is clearly observable. The nucleation of $TiO_2$- and $ZrO_2$-bearing seeds has been previously shown to induce a heterogeneous distribution of other chemical species in the glass matrix at the nanoscale,[35-39] possibly affecting the composition of the subsequently forming Qss crystals. Moreover, an overall reduction in the lattice parameters of Qss was observed in situ during isothermal ceramization of LAS glass-ceramics and connected to a gradual Si-enrichment of the crystals.[40] It is therefore possible that the impact of crystallization additives on the initial glass composition during nucleation may be responsible for the higher scattering of the structural parameters of Qss in glass-ceramics, if one neglects other possible sources of uncertainty.

As for the observed inversion from HQss to LQss during cooling at cryogenic temperatures, it exhibited a strikingly

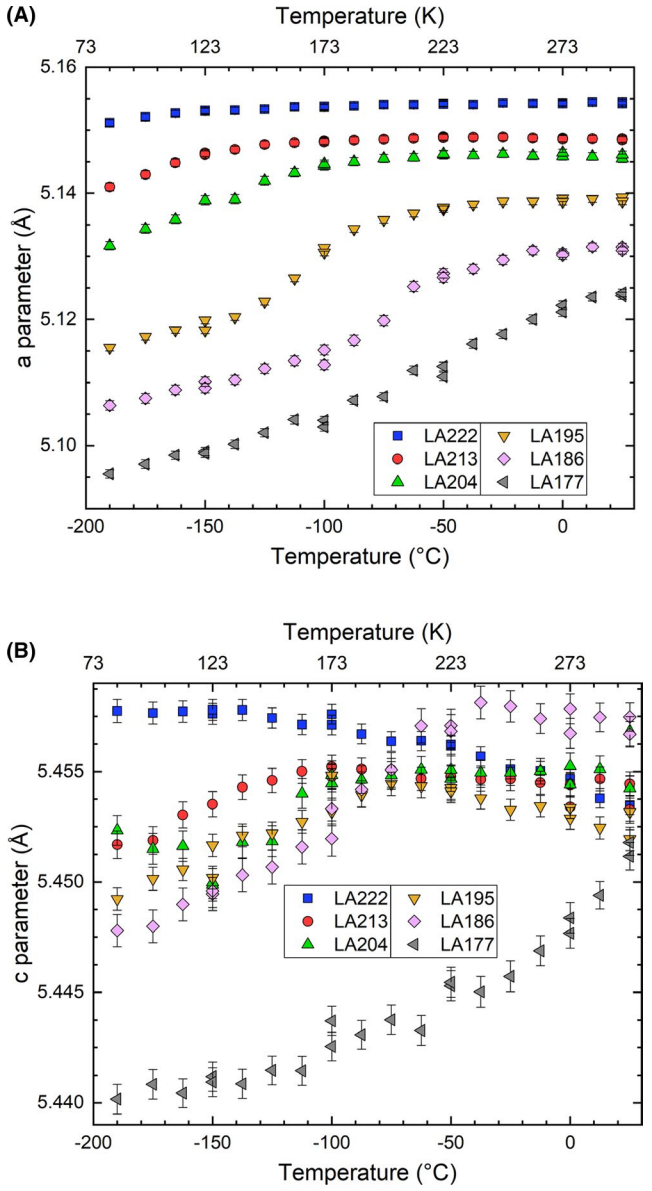


**FIGURE 4** Lattice parameters of Qss determined in situ at cryogenic temperatures (down to −190°C) in all analyzed LAS samples. If not indicated, error bars are smaller than the depicted symbols [Color figure can be viewed at wileyonlinelibrary.com]

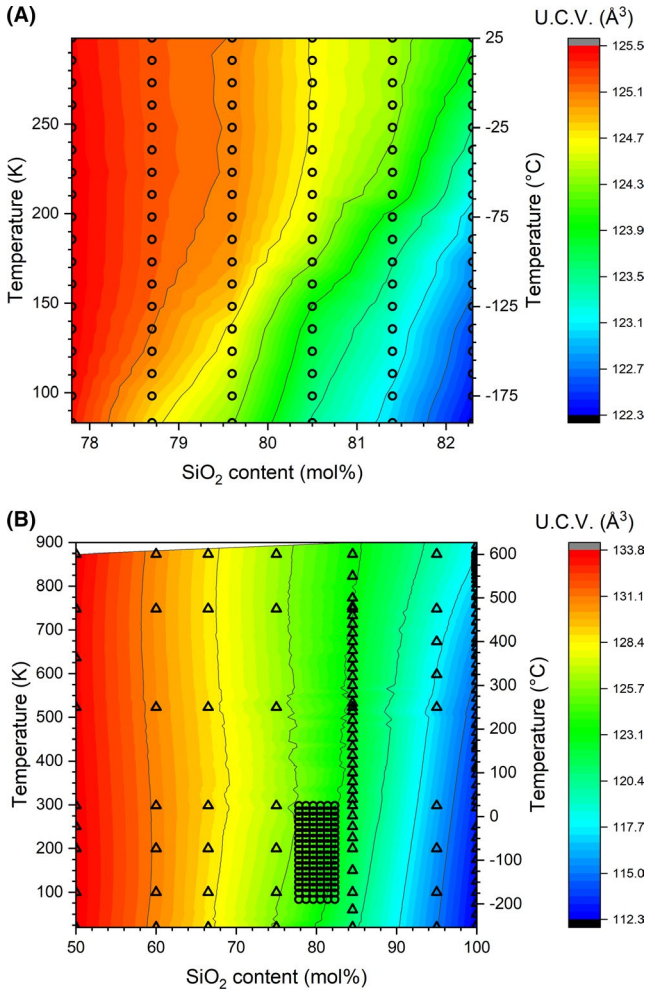


**FIGURE 5** Plot of the unit cell volume (UCV) of Qss as a function of temperature and nominal $SiO_2$ content: (A) within the range investigated by this study and (B) combining our data (open circles) to the ones from previous literature sources (open triangles[17,30]) [Color figure can be viewed at wileyonlinelibrary.com]

gradual character, in agreement with previous reports.[4,10,17,41] It is apparent that the graphically derived critical inversion temperatures $T_c$ constitute merely representative value; this is also manifested by the normalized variation in the unit cell volumes plotted in Figure 6, showing no abrupt transitions. In the past, a region of coexistence of LQss and HQss in the phase transformation range had been postulated based on the assumed higher solubility of Al + Li in the HQss structure.[41] However, no systematic splitting or broadening of diffraction peaks could be resolved within this work. Therefore, the sluggishness of the phase transformation at the studied cryogenic temperatures might be simply attributed to kinetic constraints in a single-phase material.

The general understanding of the α-β inversion in pure quartz has evolved since its first observation by Le Châtelier at the end of the XIX century[42]: it is today pictured as the combination of a first-order and a second-order transition, involving the occurrence of an incommensurately modulated

**TABLE 4** Critical inversion temperature $T_c$ of Qss in the studied samples, as determined from XRD at cryogenic temperatures; numbers in parentheses provide the uncertainty of the last digit

| Sample | Nominal $SiO_2$ (mol%) | $T_c$ (°C) |
|---|---|---|
| LA222 | 77.8 | −154(5) |
| LA213 | 78.7 | −132(5) |
| LA204 | 79.6 | −94(5) |
| LA195 | 80.5 | −81(5) |
| LA186 | 81.4 | −48(5) |
| LA177 | 82.3 | 11(7) |

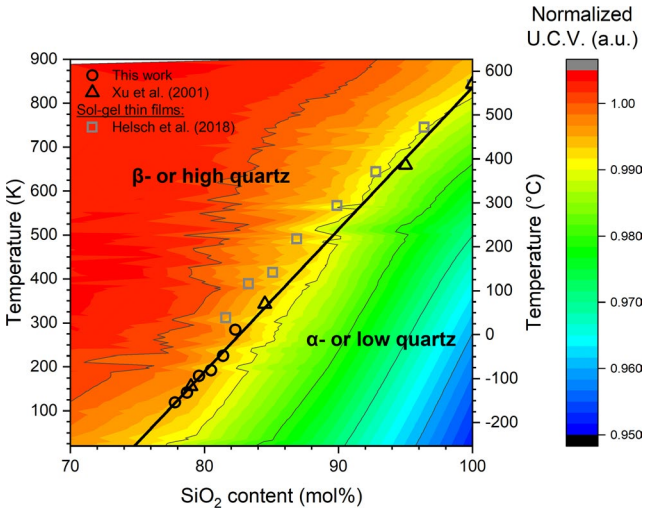


**FIGURE 6** Interpolated phase diagram for the α-β (or low-high) transition in Li-stuffed Qss as a function of temperature and nominal $SiO_2$ content (data from 17 and this work). In the background, the variation in the unit cell volume of the crystals is reported (UCV), after normalizing it by the maximum value recorded during the measurements (original data in Figure 5B). Critical temperatures $T_c$ obtained previously in sol-gel derived thin films[18] are indicated for comparative purposes. Error bars are smaller than the depicted symbols [Color figure can be viewed at wileyonlinelibrary.com]

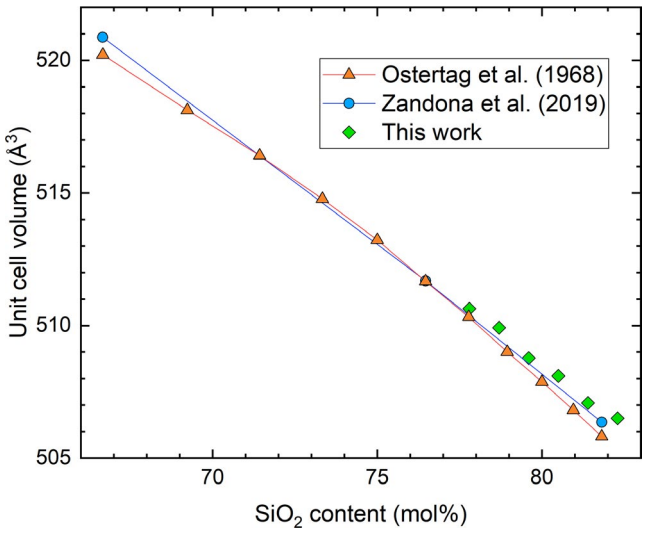


**FIGURE 7** Unit cell volumes of Kss obtained in the samples analyzed within this work, plotted as a function of the nominal $SiO_2$ content of the crystals and in comparison with available literature references[22,34]; error bars are smaller than the depicted symbols [Color figure can be viewed at wileyonlinelibrary.com]

intermediate phase over the span of approximately 1.3°C.[16] In addition, recent investigations have related this transformation to the structural response to thermally induced low-frequency, high-amplitude vibrational modes.[43] It is indeed not unlikely that the interpretation of the LQss-HQss inversion in the LAS compositional system may also be enhanced by future detailed structural analyses performed in situ, quite surpassing the scope of this study.

## 5 | CONCLUSIONS

The potential of a laboratory-based analytical equipment for the investigation of phase transformations at cryogenic temperatures has been demonstrated within this work. The linear dependence from composition of the α-β inversion temperature in Qss phases could be confirmed in the LAS compositional system: in combination with previous literature sources, it allowed the compilation of a comprehensive phase diagram for this transition.

## ACKNOWLEDGMENT

The authors kindly thank the company Schott AG, Mainz (Germany) for providing the glass samples. Open access funding enabled and organized by Projekt DEAL. [Correction added on August 20, 2020 , after first online publication: Projekt Deal funding statement has been added.]

## ORCID

*Alessio Zandona* https://orcid.org/0000-0003-0091-9546

## REFERENCES

1. Buerger MJ. The stuffed derivatives of the silica structures. Am Miner. 1954;39:600–14.
2. Bragg WL, Gibbs RE. The structure of α and β quartz. Proc R Soc Lond A. 1925;109:405–27.
3. Winkler HGF. Synthese und Kristallstruktur des Eukryptits, LiAlSiO4. Acta Cryst. 1948;1:27–34.
4. Hummel FA. Thermal expansion properties of some synthetic lithia minerals. J American Ceramic Society. 1951;34:235–9.
5. Stookey SD. Catalyzed Crystallization of Glass in Theory and Practice. Ind Eng Chem. 1959;51:805–8. https://doi.org/10.1021/ie50595a022
6. Bach H. Low thermal expansion glass ceramics. Springer-Verlag Berlin Heidelberg; 1995.
7. Beall GH. Design and properties of glass-ceramics. Annu Rev Mater Sci. 1992;22:91–119.
8. Roy R, Roy DM, Osborn EF. Compositional and stability relationships among the lithium aluminosilicates: eucryptite, spodumene, and petalite. J American Ceramic Society. 1950;33:152–9.
9. Henglein E. Zur Kenntnis der Hochtemperatur-Modifikation von Lithium-Aluminium-Silikaten. Fortschr Min. 1956;34:40–3.
10. Petzoldt J. Metastabile Mischkristalle mit Quarzstruktur mit Oxidsystem $Li_2O$-MgO-ZnO-$Al_2O_3$-$SiO_2$. Glastechn Ber. 1967;40:385–96.
11. Ray S, Muchow GM. High-quartz solid solution phases from thermally crystallized glasses of compositions ($Li_2O$, MgO)·$Al_2O_3$·n$SiO_2$. J Am Ceram Soc. 1968;51:678–82.
12. French BM, Jezek PA, Appleman DE. Virgilite; a new lithium aluminum silicate mineral from the Macusani glass, Peru. American Mineralogist. 1978;63:461–5.
13. Li C. The crystal structure of $LiAlSi_2O_6$ III (high-quartz solid solution). Zeitschrift Für Kristallographie - Crystal Mater. 1968;127:327–48.
14. Xu H, Heaney PJ, Beall GH. Phase transitions induced by solid solution in stuffed derivatives of quartz: A powder synchrotron XRD study of the $LiAlSiO_4$-$SiO_2$ join. Am Miner. 2000;85:971–9.

15. Li C-T. The role of lithium in stabilizing some high-temperature silica phases. Zeitschrift Für Kristallographie - Crystal Mater. 1973;138:216–36.
16. Heaney PJ, Veblen DR. Observations of the α-β phase transition in quartz: A review of imaging and diffraction studies and some new results. Am Miner. 1994;76:1018–32.
17. Xu H, Heaney PJ, Navrotsky A. Thermal expansion and structural transformations of stuffed derivatives of quartz along the $LiAlSiO_4$–$SiO_2$ join: a variable-temperature powder synchrotron XRD study. Phys Chem Miner. 2001;28:302–12.
18. Helsch G, Deubener J, Rampf M, Dittmer M, Ritzberger C. Crystallization and quartz inversion temperature of sol-gel derived LAS solid solutions. J Non-Cryst Solids. 2018;492:130–9.
19. Salje E, Bismayer U, Wruck B, Hensler J. Influence of lattice imperfections on the transition temperatures of structural phase transitions: The plateau effect. Phase Transitions. 1991;35:61–74.
20. Beall GH, Karstetter BR, Rittler HL. Crystallization and chemical strengthening of stuffed beta-quartz glass-ceramics. J American Ceramic Society. 1967;50:181–90.
21. Schreyer W, Schairer J. Metastable solid solutions with quartz-type structures on the join $SiO_2$–$MgAl_2O_4$. Zeitschrift Für Kristallographie. 1961;116:60–82.
22. Zandona A, Rüdinger B, Hochrein O, Deubener J. Crystallization sequence within the keatite solid solution – cordierite mixed compositional triangle with $TiO_2$ as nucleating agent. J Non-Cryst Solids. 2019;505:320–32.
23. Ray S. Study of ordering in high-quartz solid solutions by substitutions affecting superlattice reflections. J Am Ceram Soc. 1973;56:42–5.
24. Schulz H, Muchow GM, Hoffmann W, Bayer G. X-ray study of Mg-Al silicate high-quartz phases. Zeitschrift Für Kristallographie - Crystal Mater. 1971;133:91–109.
25. Sternitzke M, Müller G. Crystal structure and thermal expansion of quartz-type aluminosilicates. J Mater Sci. 1991;26:3051–6.
26. Xu H, Heaney PJ, Yu P, Xu H. Synthesis and structure of a stuffed derivative of α-quartz, $Mg_{0.5}AlSiO_4$. Am Miner. 2015;100:2191–8.
27. Kwei GH, Lawson AC, Billinge SJL, Cheong SW. Structures of the ferroelectric phases of barium titanate. J Phys Chem. 1993;97:2368–77.
28. Wang K, Reeber RR. The role of defects on thermophysical properties: thermal expansion of V, Nb, Ta, Mo and W. Mater Sci Eng R Rep. 1998;23:101–37.
29. Taylor D. Thermal expansion data: III sesquioxides, $M_2O_3$, with the corundum and the A-, B- and C-$M_2O_3$ structures. Trans J Br Ceramic Society. 1984;83:92–8.
30. Carpenter MA, Salje EKH, Graeme-Barber A, Wruck B, Dove MT, Knight KS. Calibration of excess thermodynamic properties and elastic constant variations associated with the α ↔ β phase transition in quartz. Am Miner. 1998;83:2–22.
31. Xu H, Heaney PJ, Navrotsky A, Topor L, Liu J. Thermochemistry of stuffed quartz-derivative phases along the join $LiAlSiO_4$-$SiO_2$. Am Miner. 1999;84:1360–9.
32. Nakagawa K, Izumitani T. Metastable phase separation and crystallization of $Li_2O{\cdot}Al_2O_3{\cdot}SiO_2$ glasses: determination of miscibility gap from the lattice parameters of precipitated β-quartz solid solution. J Non-Cryst Solids. 1972;7:168–80.
33. Loewenstein W. The distribution of aluminum in the tetrahedra of silicates and aluminates. Am Miner. 1954;39:92–6.
34. Ostertag W, Fischer GR, Williams JP. Thermal expansion of synthetic β-spodumene and β-spodumene—silica solid solutions. J Am Ceram Soc. 1968;51:651–4.
35. Bhattacharyya S, Höche T, Jinschek JR, Avramov I, Wurth R, Müller M, et al. Direct evidence of Al-Rich layers around nanosized $ZrTiO_4$ in glass: putting the role of nucleation agents in perspective. Cryst Growth Des. 2010;10:379–85.
36. Zandona A, Patzig C, Rüdinger B, Hochrein O, Deubener J. $TiO_2$(B) nanocrystals in Ti-doped lithium aluminosilicate glasses. J Non-Cryst Solids: X. 2019;2:100025.
37. Kleebusch E, Patzig C, Krause M, Hu Y, Höche T, Rüssel C. The formation of nanocrystalline $ZrO_2$ nuclei in a $Li_2O$-$Al_2O_3$-$SiO_2$ glass – a combined XANES and TEM study. Sci Rep. 2017;7:10869.
38. Kleebusch E, Patzig C, Höche T, Rüssel C. The evidence of phase separation droplets in the crystallization process of a $Li_2O$-$Al_2O_3$-$SiO_2$ glass with $TiO_2$ as nucleating agent – An X-ray diffraction and (S) TEM-study supported by EDX-analysis. Ceram Int. 2018;44:2919–26.
39. Di Genova D, Zandona A, Deubener J. Unravelling the effect of nano-heterogeneity on the viscosity of silicate melts: implications for glass manufacturing and volcanic eruptions. J Non-Cryst Solids. 2020;545:120248.
40. Dressler M, Rüdinger B, Deubener J. An in situ high-temperature X-ray diffraction study of early-stage crystallization in lithium alumosilicate glass-ceramics: an in situ high-temperature X-ray diffraction study. J Am Ceram Soc. 2011;94:1421–6.
41. Keith ML, Tuttle OF. Significance of variation in the high-low inversion of quartz. Am J Sci Bowen. 1952;203–80.
42. Le Chatelier H. Sur la dilatation du quartz. Bulletin de la Société française de Minéralogie. 1890;13(3):1890.
43. Tucker MG, Keen DA, Dove MT. A detailed structural characterization of quartz on heating through the α-β phase transition. Mineral Mag. 2001;65:489–507.

**How to cite this article:** Zandona A, Helsch G, Deubener J. Inversion of quartz solid solutions at cryogenic temperatures. *J Am Ceram Soc*. 2020;103:6630–6638. https://doi.org/10.1111/jace.17393